Cu^{2+} ions implanted porous titania for efficient dye sensitized solar cells

M. Irfan[a], M. I. Khan[a,*], I. Ul-Haq[a], M. Amam[a], Ihab M. Moussa[b], S. Mumtaz[c]
[a]*Department of Physics, The University of Lahore, 53700, Pakistan*
[b]*Department of Plant Production, College of Food & Agriculture Sciences, King Saud University, P.O. Box 2460, Riyadh 11451, Saudi Arabia*
[c]*Electrical and Biological Physics, Kwangwoon University, Seoul, 01897, South Korea*

In the quest to unlock the remarkable potential of nanotechnology, the sol-gel method was employed to craft a porous TiO_2 nanostructured film, meticulously deposited onto FTO glass substrates. This endeavor marked a significant leap as a controlled bombardment of Cu ions, accelerated at 700 keV, at varying flux rates of $2x10^{13}$, $2x10^{14}$, and $2x10^{15}$ ions/cm² was introduced to these ingeniously engineered films. A comprehensive assessment of these nanocrystalline TiO_2 structures, both before and after Cu^{+2} ion irradiation, revealed a fascinating array of results. he anatase tetragonal structure's permanence was validated by X-ray diffraction (XRD), which improved the material's stability and integrity. In the present study, an interesting observation was made that band edges show a dynamic behavior in Cu-irradiated samples in UV-Vis spectroscopy. At $2x10^{14}$ ions/cm^2, the phenomena peaked, revealing an intriguing redshift and an exceptionally low band gap value of 3.39 eV. In photoluminescence spectra, the peaks corresponding to the lattice defects show a significant reduction when the flux of the Cu ions on TiO_2 is adjusted to 2 x 10^{14} ions/cm^2. It is an indication that film quality and purity have improved. This arrangement for photoanode modification helps in the development of dye-sensitized solar cells with tremendous characteristics. The fabricated device with this novel approach results in high values of open circuit voltage (Voc), short circuit current density (Jsc), fill factor (FF), and maximum photoconversion efficiency of 5.10%. These findings indicate a new era of possibilities in the field of renewable energy, since these nanostructured materials have the ability to significantly alter the solar field.

(Received February 5, 2024; Accepted July 3, 2024)

Keywords: Sol-gel, Cu, Ions irradiation, TiO_2 nanostructured film, Dye-sensitized solar cell

1. Introduction

The current energy demands are fulfilled by fossil fuels like raw oils, coal, and natural gas. The need for energy to support daily routines is growing along with the population's fast growth. The overuse of fossil fuels has a negative impact on the environment because of air pollution and global warming [1]. The rapid utilization of fossil fuels depletes the earth's reservoir and will ultimately end. These fossil fuels are the non-renewable energy resources. So, there is a need to substitute these non-renewable energy resources to reduce these adverse environmental effects and fulfill future energy needs. There are many renewable energy resources, and solar energy is the best of all exciting resources. It has been estimated that the utilization of only 0.1 % of solar energy reaching Earth can meet the world energy demand for a year by using solar cells with 10% photoconversion efficiency [2]. The well-known Si-based solar cells are expensive, as their complicated manufacturing process, requirement of highly purified raw material and small lifespan are significant barriers to their adoption. These DSSCs can effectively replace traditional silicon-based solar cells. The fabrication of the dye-sensitized solar cell by Grätzel and O'Regan was a breakthrough, and after this discovery, efforts were started to obtain high-efficiency photoconversion efficiency [3, 4] and till today 15.2% efficiency has been achieved [5]. The dye-sensitized solar cells have been thoroughly investigated because of their easy manufacturing process,

* Corresponding author: muhammad.irfan6252@gmail.com
https://doi.org/10.15251/JOR.2024.204.417

lightweight, offer less toxicity and low-cost raw materials, increases their acceptance in the energy production technology [3]. The manufacturing cost of the dye-sensitized solar cells (DSSCs) is 30 % less than traditional p-n junction solar cell technology [6-8]. These cells even work in the cloudy atmosphere, and this property makes them suitable for indoor applications as well. The major component of dye-sensitized solar cells is the photoanode. The well-known material utilized for photoanode fabrication is TiO_2. It is the most suitable semiconducting material for the DSSCs fabrication because its Fermi energy level is ideal for capturing electrons generated via photolysis of the dye molecules [9].

One of TiO_2's drawbacks is its high band gap which limits its suitability for visible light sensitivity and instead makes it suitable mainly for ultraviolet absorption. This ultra-violet region of the electromagnetic spectrum is only 2 to 3 % of the sunlight [10-12]. The high recombination rate of electron-hole pairs caused by TiO_2's large band gap value lowers the efficiency of DSSC [13]. The device performance can be improved by tuning band gap value of TiO_2 and increasing its sensitivity for visible region. It has been reported that metal doping reduces carrier recombination, thus improving its performance. But doping process involves complex chemical reactions, and the formation of by-products becomes problematic [14]. The physical irradiation of high-energy ion beam implantation can address this issue. It has been reported that ion irradiation on the TiO_2 film has modified it successfully both physically and chemically [15]. In this study, we report utilizing Cu ions implantation on the TiO_2 material at various fluency rates. This ions irradiation improves the photovoltaic traits of the dye-sensitized solar cells (DSSCs). Because of its easy accessibility in the earth's and having high electronic conductivity, copper is a desirable metal for irradiating DSSCs' TiO_2 semiconductor photoanode. TiO_2's broad band gap may be reduced as a result of the Cu ion in TiO_2 being irradiated. Cu-irradiated TiO_2 can make it easier for photo-generated charge carriers to pass through, increasing the short circuit current density (J_{sc}), thus increases the photoconversion efficacy of DSSC. We also highlighted how the open circuit voltage V_{oc} improves by Cu inclusion in TiO_2 by the close movement of band edges of conduction and valance bands and the absorption band spectrum shifting towards the visible region [16].

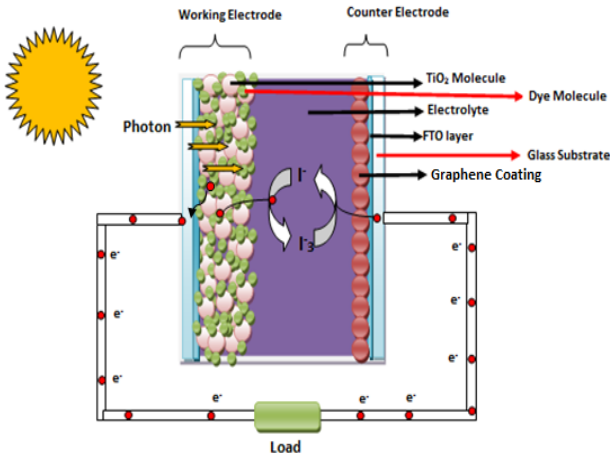

Fig. 1. Schematic view of DSSCs.

Because it addresses a significant issue with dye-sensitized solar cells, this research is extremely important for photovoltaics and renewable energy. The primary objective was to enhance the efficiency of these solar cells by mitigating the recombination rate and elevating current density, crucial factors in their performance. What sets this work apart is the novel approach of ion implantation, specifically employing Cu ions, to achieve this optimization.

Usually, a chemical method is used for the doping of Cu in TiO_2, resulting in the introduction of additional impurities in the synthesized sample, which ultimately reduces the efficiency of DSSCs.

On the other hand, the ion implantation method is better than the chemical method as it guarantees that no other element other than Cu will be added to the TiO_2 crystal lattice. This precise insertion of Cu into TiO_2 enables the photoanode to have a positive impact on the efficiency of the fabricated dye-sensitized solar cell. Remarkable results are obtained by the irradiation process, and the maximum level of crystallinity and current density were obtained in the fabricated device at a flux rate of $2x10^{14}$ ions/cm^2 by precisely regulating the energy of fluency of Cu ions at 700 keV. This achievement not only illustrates the significance of the present study but also establishes that nanotechnology and the ion implantation process can be the breakthrough in solar cell technology in renewable energy applications.

2. Experimentation

The sol-gel technique was used for generating the nanostructured TiO_2 material. In this method, precursors are Titanium (IV), Isopropoxide (TTIP), Ti [OCH $(CH_3)_2]_4$ bought from Sigma Aldrich, and Ethylene Glycol (EG) distilled water and HNO_3 acid. 24 ml of TTIP is taken in a beaker, and ethylene glycol is mixed with TTIP with continuous stirring to obtain a homogeneous solution. HNO_3 diluted with distilled water is incorporated in the above-prepared solution, initiating the hydrolysis of TTIP and forming TiO_2. As the process continues, a gel will grow over time. Four pieces of 2.5 x 2.5 cm^2 of FTO substrate are immersed in the above-made gel to obtain thin films. To eliminate the solvent and improve the crystal characteristics, the coated FTO substrate with TiO_2 film is dried and annealed at 450 ^{0}C for two hours after the dip-coating procedure. Three films were exposed to Cu ion radiation at flux of 2 x 10^{13}, 2 x 10^{14} and 2 x 10^{15} ions/cm^2, whereas one film was left pure.

2.1. Preparation of the DSSCs

The developed photoanodes with fluence rates of $2x10^{13}$, $2x10^{14}$, and $2x10^{15}$ ions/cm^2 were exposed to Cu^{2+} ions for 20 hours before being dipped into N719 dye. One of these photoanodes was used to seal the Pt coated counter electrode, and the electrode itself was given a tiny hole punched in it. Iodide/tri-iodide is inserted through this hole to serve as the electrolyte between these electrodes, and the hole is then sealed. With this technique, four cells were created. One was pure, and three were Cu-irradiated. A schematic of these manufactured cells is witnessed in Figure 1. The assembled cells were characterized by J-V measurement to determine their efficiency.

2.2. Photovoltaic characterization of the DSSCs

By means of an ABET Technologies solar simulator, J-V curves for the dye-sensitized solar cells at 1000Wm^{-2} (1.5AM simulated sunshine) were obtained in order to gather information on the short circuit current density, open circuit voltage, and fill factor. Using a Keithley-source meter, model 2601, the output voltage and current density values for the cells are recorded.

2.3. Characterization

Using a German q-q STOE X-Ray diffractometer operating at room temperature, we obtain an XRD pattern for the samples under investigation for their phase and structural analysis. X-Rays are obtained from Cu-K_α source. The operating voltage was adjusted to 40 kV, and the current was 30 mA. The measurements were made with a 0.040-step resolution and a 2θ-80θ-scan-angle range. Using a BMS 2800 UV-Vis spectrophotometer the data was obtained in the wavelength range of 300 nm to 800 nm. $BaSO_4$ powder was used as the standard reference for getting the required data.

3. Result and discussion

3.1. XRD analysis

In the diffractogram, the most intensive (101) peak is observed at $2\theta = 25.37^0$ for the pure sample, whereas, as for the Cu^{2+} irradiated samples, the peak (101) are observed at $2\theta = 25.31^0$,

25.26^0, 25.22^0 and 25.31^0 at fluence rates of 2 x 10^{13}, 2 x 10^{14} and 2 x 10^{15} ions/cm^2 respectively. JCPDS card No. 21-1272 shows that the diffractogram's peaks are all identified as being in the TiO_2 anatase phase. Anatase works better than other phases because it permits greater dye absorption [17]. A low concentration of irradiated Cu^{2+} may cause an absence of apparent modification when compared with XRD patterns of pure TiO_2 samples. Due to the extremely low concentration, no copper peaks can be seen in the XRD of the irradiated Cu thin films.

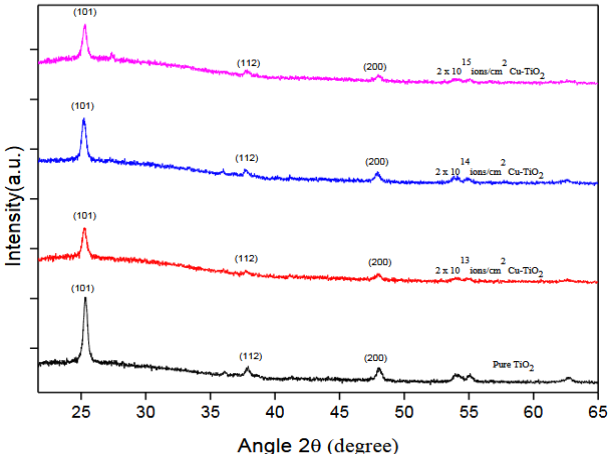

Fig. 2. XRD patterns of pristine and Cu $^{2+}$ irradiated TiO_2 films.

The absence of secondary or impurity peaks corresponding to the Cu in the diffractogram demonstrates that Cu^{2+} successfully substituted on Ti^{4+} sites despite aggregating interstitially[18, 19]. The shifting of the peaks towards a lower angle at 2 x 10^{13} and 2 x 10^{14} ions/cm^2 flux of Cu ions is noticed, which can be attributed to the distortion in the crystal due to the Cu-irradiation process. Cu^{2+} (0.65Å) is a higher ionic radius atom thanTi^{4+} (0.61Å); thus, lattice expansion is caused by the insertion of Cu^{2+} ions for Ti^{4+} in the TiO_2 crystal lattice may contribute to this shift in XRD [20].

When the fluency rate increased from 2x10^{14} ions/cm^2, peak shifting was seen, advancing towards a higher angle. This may be due to a higher level of oxygen vacancies as Cu^{2+} concentration in TiO_2 increases, and the crystal gets contracted [21] also, the anatase peak shifts towards a higher angle, showing evidence of efficient lattice stressing [22]. The peak intensity in the diffractogram decreases with the Cu^{2+} irradiation process. This reduction is linked to the strain and lattice disorder produced in the TiO_2 lattice [23]. The peak broadening is observed when the Cu^{2+} ions in the TiO_2 crystal lattice increases. The crystalline quality decreases due to substituting higher ionic radii Cu^{2+} atom with smaller ionic radii Ti^{4+} atoms. The peak broadening is observed by FWHM, which is utilized to calculate the crystallite size.

We utilized the Debye-Scherrer relation as given below for the calculation of average crystallite size D for the (101) peak

$$D = \frac{0.9\lambda}{\beta\cos\theta} \tag{1}$$

Here β is representing full width at half maximum, the wavelength is expressed by λ (1.5418 Å) from source CuK_α, where angle θ is the Bragg's angle. The crystallite size of pristine and Cu^{2+} irradiated-TiO_2 at fluence rates of 2x10^{13}, 2x10^{14} and 2x10^{15} ions/cm^2 are 22.72 nm, 22.22 nm, 21.82 and 22.13 nm respectively. Lowering in crystallite size is observed on account of an increase in the Cu^{2+} ions in the TiO_2 lattice up to 2x10^{14} ions/cm^2. The particle size of TiO_2 reduces by its suppression of condensation and crystallization on account of the induction of Cu^{2+} ions in TiO_2. Thus the presence of Cu in TiO_2 hinders its growth, so crystallinity decreases [22].

Additionally, the reduction in crystallite size can be linked to the retarding force operating on the grain boundaries. Increasing Cu^{2+} concentration in the TiO_2 system will gradually reduce Ti concentration in it. The reduction of diffusivity in TiO_2 suppresses grain growth after Cu^{2+} irradiation [24]. The replaced Cu ions also act as a decelerating force on the grain boundaries. If the presence of Cu^{2+} has a more worth noting retarding effect on the TiO_2 grain boundaries than a driving effect from Ti^{4+}, the grain boundary's ability to move will be constrained [25, 26]. Consequently, when the concentration of Cu rises, the crystallite size steadily decreases [23]. In general, peak width grows as crystallite size decreases.

The square of the crystallite size, which is determined by the following relation, is inversely proportional to the dislocation line density.

$$\delta = \frac{1}{D^2} \tag{2}$$

The quantity of dislocations in the crystalline material is given by dislocation line density **δ**. This shows that crystal imperfection decreases with an increase in the crystallite size. The small value of the dislocation line density is the indication that conductivity for the flow of charges has been increased as the resistance put up in the charge flow along the grains decreases, which increases smooth charge flow [27]. A decrease in grain size induces more disorder in the system. Therefore, 1/D describes disorder in the system. As the ionic radius of Cu^{2+} is greater than Ti^{4+}, thus more disorder will be introduced by the Cu ions insertion in TiO_2 [23].

For the calculation of the lattice parameter of tetragonal symmetry, the following relation is utilized

$$\frac{1}{d^2} = \frac{h^2 + k^2}{a^2} + \frac{l^2}{c^2} \tag{3}$$

(hkl) expresses Miller indices, d expresses the interplanar spacing, and a, b, and c representing the lattice parameters. Volume of tetragonal symmetry is determined by using the following relation [28]

$$V = (a^2 \times c) \tag{4}$$

The volume of pure and Cu- irradiated TiO_2crystal lattice at fluence rates of $2x10^{13}$, $2x10^{14}$ and $2x\ 10^{15}$ ions/cm^2 are 136.429 Å^3, 138.765 Å^3, 138.763 Å^3 and 135.956 Å^3 respectively. The expansion of the lattice is seen which results in the shifting of the peak towards a lower angle and then contracts when the fluency rate increases from $2x10^{14}$ ions/cm^2. This decrease in the volume was observed due to the re-crystallization process in the presence of Cu^{2+} [29] and also due to the generation of oxygen related defects in TiO_2 [21].

The value c axis of pristine and Cu- irradiated TiO_2 crystal at fluence rates of $2x\ 10^{13}$ ions/cm^2, $2x\ 10^{14}$ ions/cm^2 and $2x\ 10^{15}$ ions/cm^2 are 9,508 Å, 9.681 Å, 9.635 Å and 9.460 Å respectively as shown in Table 1. It is evident that the values of a = b and c somewhat increases as the Cu^{+2} concentration rises. Cu atoms' capacity to replace Ti atoms in the TiO_2 system is affected because the Cu^{+2} ionic radius higher than the Ti^{+4} ionic radius, increasing the samples' lattice parameters [30].

Table 1. Interplanar spacing and lattice characteristics of pure and Cu-irradiated TiO_2 films at varying fluency rates.

Sample	2θ	FWHM B	a(Å)	c(Å)	Interplanar spacing d(Å)	Crystallite size D (nm)	Volume V (Å)^3
Pure TiO_2	25.37	0.3743	3.788	9.508	3.511	22.7286	136.429
Cu-irradiated-TiO_2 with 2 x 10^{13} ions/cm^2	25.26	0.3828	3.786	9.681	3.526	22.2217	138.765
Cu-irradiated-TiO_2 with 2 x 10^{14} ions/cm^2	25.22	0.3897	3.795	9.635	3.531	21.8266	138.763
Cu-irradiated-TiO_2 with2 x 10^{15} ions/cm^2	25.31	0.3843	3.791	9.460	3.519	22.1371	135.956

3.2. Optical properties

With the help of optical absorbance, we can easily determine optical properties like band gap value, refractive index, extinction coefficient, absorbance etc., of the photoanode used for DSSCs fabrication.

3.2.1. Band gap energy

Band gap energy is an essential property of materials, particularly in solid-state physics and semiconductor technology, as it describes the electrical and optical characteristics of the material.

It has been noted that introducing Cu^{2+} into TiO_2 lowers the material's Eg because the energy band gap of TiO_2 is being filled with impurity energy levels. As a result, the conducting band shifts slightly downward.

[31]. Tauc's relation is given below for determining the band gap energy

$$(\alpha h\nu) = A(h\nu - E_g)^m \quad (5)$$

In the equation above, m is a constant depends upon the electronic transition, and photon energy given by hν and **α** absorption coefficient. By projecting Tauc's plot towards the energy axis, as illustrated in Figure 3, it is possible to calculate the band gap energy value. At flow rates of $2x10^{13}$, $2x10^{14}$, and $2x10^{15}$ ions/cm^2, the band gap thus obtained for pure and Cu^{2+} irradiated TiO^2 is 3.49 eV, 3.43 eV, 3.39 eV, and 3.40 eV, respectively. At 700 KeV accelerated energy, the irradiation Cu^{+2} implant themselves into the crystal lattice, causing the neighboring atoms to rearrange themselves to balance the charge deficient state. To maintain charge neutrality, oxygen vacancies are generated, causing Eg to gradually decrease as the TiO_2 lattice's concentration of Cu ions rises [20, 22]. Since the substitution of Ti^{4+} with Cu ions, which is in the +2 state induces oxygen vacancies for the charge compensation, a change in crystallinity is observed. The band gap of the material develops impurity states as a result of the extra Cu ions trapped in the grain boundaries. The density of these Cu-induced impurity levels rises with rising Cu ions fluency rates, which causes the Eg to decrease [32]. The introduction of two lone pair states above the valance band of TiO_2 by the Cu^{+2} ions in the TiO_2 crystal is another cause leading the band gap energy to decrease [17, 33]. The irradiation method may result in such efficient band gap lowering, which could reduce Fermi levels and increase the activity of the synthesized samples [34]. When the fluency rate of Cu^{+2} on TiO_2 increased from $2x10^{14}$ ions-cm^{-2}, the excess Cu atoms did not occupy the appropriate lattice locations to contribute to the free carrier concentration but instead enhanced the structure's disorder, which widened the band gap, which is noticed at flow rate of $2x10^{15}$ ions-cm^{-2} [35]. This region's dropping atomic density causes the Cu irradiation thin film's band gap energy to rise even further. In the interstitial regions, this mechanism leads to a rise in the amorphous phase, the development of disorder,

and Ti^{4+} ion transport. The band gap widens due to the increased disorder in the structure [36].

As illustrated below, the band gap energy is inversely proportional to the wavelength of the absorption band gap [19].

$$Eg = \frac{1240}{\lambda} eV \quad (6)$$

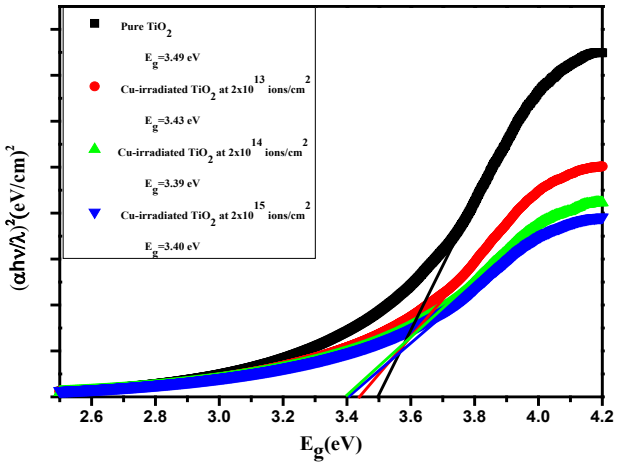

Fig. 3. Energy gap values of pristine and Cu-irradiated TiO_2 film at various fluency rates.

3.2.2. Absorbance

The absorption band spectrum of Cu^{2+}-irradiated samples extends towards longer wavelength side of electromagnetic spectrum compared to the pure TiO_2 sample due to formation of intermediate energy levels. The highest absorption levels are caused by electrons being transit from valance to conduction band. O 2p states make up the valance band of TiO_2, whereas Ti 3d states make up the conduction band. Thus, peak absorption is seen as a result of the electron transfer from O 2p to Ti 3d. Charge transfer from valance band VB having O 2p states to Cu (II) present in TiO_2 results in the shifting absorption band spectrum towards the higher wavelength side, which is observed at the interface. Therefore, the optical absorption change and band gap reduction are caused by defect centres created when Cu^{2+} atoms replace Ti^{4+} atoms.

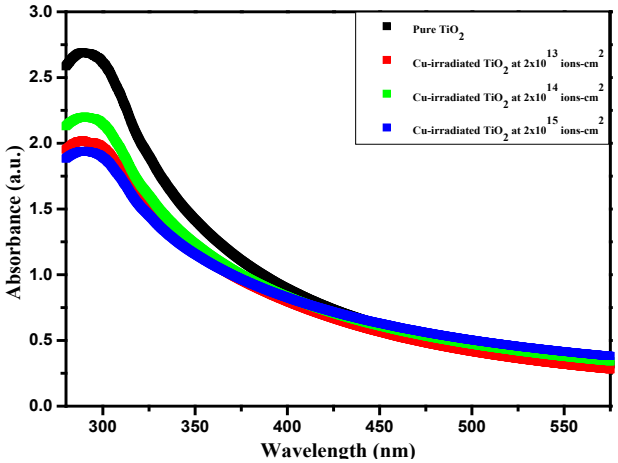

Fig. 4. Absorbance versus wavelength of pure TiO_2 film and irradiated with Cu ions.

Cu-irradiated TiO_2's absorption coefficient improves as the visible region's absorption peaks get broader; absorption decreases as wavelength increases. This shows how copper helps extend absorption light spectra toward longer wavelength regions. The transition of photogenerated in the TiO_2 conduction band was made more accessible by the introduction of the impurity energy level below and close to the conduction band. This results in the absorption peak shifting towards the visible region. Thus a quick charge transfer, there is less recombination chance of charges [37, 38]. The decrease in absorbance in the Cu-irradiated samples at high fluence rate can be attributed to Cu irradiation's removal of imperfections and disorder in the initially-deposited film [36].

It has been found that when pure TiO_2 and Cu^{+2}-irradiated TiO_2 are compared, the irradiated samples perform better at harvesting light. This proves that the apparent absorbance is closely correlated with the presence of Cu^{2+} in TiO_2.The oxygen vacancies are the consequences of the charge compensation process shifting optical absorption in the longer wavelength region [39].

As absorbance has an inverse relation with transmittance, thus it was discovered that transmittance decreases with increasing implanted concentration, which is caused by an increase in the amorphousness of the films exposed to radiation. Many variables, including thickness, porosity, surface roughness, and polycrystallinity, influence how well a film transmits light. Surface roughness and optical inhomogeneity of the film surface are two additional factors that affect the transmittance of the films. With higher Cu concentration in TiO_2 at fluency rate of $2x10^{15}$ ions/cm^2 the decrease in transmittance indicates an increase in the band gap, which may bring an increase in carrier mobility or carrier concentration [36].

3.2.3. Refractive index

Using the following relation, the refractive index of the pure and Cu^{+2} irradiated samples are determined [40].

$$n = \sqrt{1 + (\frac{A}{E_g + B})^2} \tag{7}$$

13.6 eV and 3.4 eV are the values of constants A and B. n is measured using the above equation for pure and Cu^{2+} irradiated samples are 2.212, 2.228, 2.238 and 2.236 at flow rates $2x10^{13}$, $2x10^{14}$ and $2x10^{15}$ ions/cm^2 respectively. The refractive index falls with increasing Cu^{2+} ions concentration but decreases when the fluency rate increases from $2x10^{14}$ ions/cm^2. The impurity in the film increases its optical characteristics, causing the film to have a high refractive index [36]. Because of the crystal's periodicity disturbance caused by the high Cu content in the TiO_2 matrix, the refractive index n of the samples increases with increasing fluency and reaches a maximum value of 2.238 at flux of $2x10^{14}$ ions/cm^2. Due to the material's higher density due to Cu addition, there is a high refractive index value. High absorption of light results from high scattering, which is caused by a high refractive index, while low refractive index values indicate excellent transparency [41]. It is clear that the refractive index value rises in tandem with an increase in Cu^{2+} concentration, showing that the films become denser. Refractive index decreases to 2.192 at a fluency rate of $2x10^{15}$ ions/cm^2, showing low packing density and the formation of a porous structure. The relatively large porosity is explained by the mismatch in lattice between the mixed phases. Furthermore, the low refractive index at higher Cu^{2+} concentrations in TiO_2 crystal lattice at $2x10^{15}$ ions/cm^2 fluency rate could result from either be related to the photon energy that is then reflected inside and trapped within the grain boundaries. This could have something to do with the crystal lattice's defects and impurities. This may also be connected to the fact that the crystal lattice contains many defects and impurities [42].

3.2.4. Band edges calculations

The driving force for photogenerated electrons in DSSCs can be calculated from the position of conduction and valance band edges of photoanode material.

The conduction and valance band positions can be computed using the subsequent relationships

$$E_{CB} = X - E_C - \frac{1}{2}E_g \tag{8}$$

in which

$$X = \frac{1}{2}(E_{EA} + E_{ion})$$

In the aforementioned relationships, Eg is the band gap energy value and E_C is the energy of free electrons on the hydrogen scale, which has a value of 4.5 eV. E_{EA} is electron affinity and E_{ion} is first Ionization Energy of the samples.

The relationship provided below can be used to calculate the valance band edge.

$$E_{VB} = E_{CB} - E_g \tag{9}$$

The calculated are given in the Table 2.

From the calculations it is clear that the absorption's band edge shifts toward long wavelengths after Cu irradiation, indicating that the Cu irradiation has decreased the band gap. Additionally, as seen in the redshift of the light absorption, the band gap energy of the Cu-irradiated sample decreases [19]. This decrease in band gap energy resulted from the conduction band edge moving downward, as shown in Figure 5. The conduction band edge usually changes synchronously with the quasi-Fermi level's equal displacement with respect to the I^{3}-/I^{-1} Fermi level. The key factor contributing to the increase in absorbance is this positive displacement of the conduction band edge.

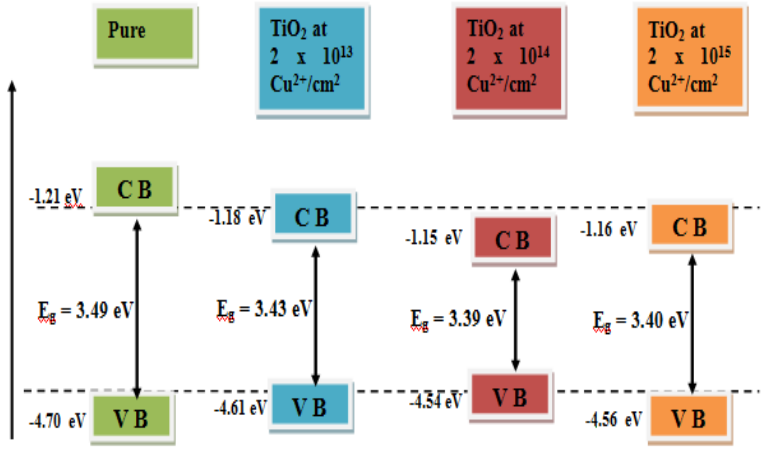

Fig. 5. Band gap edges position of pure and Cu-irradiated TiO_2 films.

However, it is evident from the examination of optical spectra that the smaller band gap of the Cu-irradiated TiO_2 sample is also a result of a positive shift in the conduction band edge. The conduction band edge shifts downward, lowering the Eg and enhancing the driving force of the excited electrons. This reduction of Eg results in an increase in the number of TiO_2 (e-) in the Cu-irradiated sample.

It is well known that when smaller-sized Ti^{4+} metal ions are replaced by bigger-sized metal Cu^{2+} ions, irradiation with metal ions distorts the lattice structure. To retain charge

neutrality, this substitution promotes the introduction of oxygen vacancies. When titania is subjected to copper radiation, Cu^{2+} ions condense on the surface or interior. As a result of the adjacent atoms being rearranged to balance the charge deficiency, the lattice is deformed. The band gap shift occurs due to the lattice's deformation and rearrangement, which changes the electronic structure [43]. Additionally, oxygen vacancies are produced as a result of small concentrations of Cu^{+2} being present in titania's lattice sites [44]. These are a result of the effect of charge compensation. The band edge position and absorption spectra of nanostructured films are altered by lattice strain and oxygen vacancies produced due to the Cu irradiation process.

Table 2. Band edge values of the pure and Cu^{+2} irradiated films for the conduction and valance bands

Sample	E_g (eV)	X (eV)	E_{CB} (eV)	E_{VB} (eV)
Pure TiO_2	3.49	5.04	-1.21	-4.70
Cu-irradiated-TiO_2 with 2 x 10^{13} ions/cm^2	3.43	5.04	-1.18	-4.61
Cu-irradiated-TiO_2 with 2 x 10^{14} ions/cm^2	3.39	5.04	-1.15	-4.54
Cu-irradiated-TiO_2 with 2 x 10^{15} ions/cm^2	3.40	5.04	-1.16	-4.56

3.3. Photoluminescence (PL) emission spectra

A process in which a substance emits light when it absorbs it from some external source is known as photoluminescence. In this process, the electrons, after absorbing light, jump to some higher energy level, which is the unstable state for that atom. It jumps again to its parent energy level with the emission of energy in the form of light, which was absorbed. This phenomenon applies to various practical applications like LEDs, fluorescence microscopy, etc.
Photoluminescence spectroscopy is also utilized for material characterizations such as organic materials, semiconductors, and nanoparticles. The spectra of the light emitted from the substance under investigation help in understanding the band structure and carrier dynamics.

The trapping and migration of the electron-hole pair in the semiconductor can be analyzed by the study of the photoluminescence spectrum obtained from that material. The photoluminescence emissions result from the impurity energy levels that are produced due to the Cu-irradiation process on TiO_2 films, thus changing their electronic structure. At various concentrations, Cu ions in TiO_2 cause peaks in PL emission spectra at various wavelengths. The emission peaks can be related to defects that are induced by the Cu presence in the crystal lattice [45]. Different forms of defects, including oxygen vacancies, can be seen in the samples' photoluminescence (PL) spectra. The green PL in TiO_2 nanomaterial is caused by oxygen vacancies [46].

Figure 6 illustrates the photoluminescence spectra of pristine, and Cu^{+2} irradiated TiO_2 samples at the fluence rates of $2x10^{13}$ and $2x10^{14}$ ions/cm^2. Four prominent peaks are noticed at 404 nm, 420 nm, 491 nm and 538 nm for all thin films. The migration of electrons between bands, from the conduction band minima to the valance band maxima, which occurs at two different sites, is the process that causes the emission peak at 404 nm. The oxygen defect-related shallow and deep trap centers and excitons resulted in the emission peaks in the visible region. The self-trapped exciton causes the emission at 420 nm. When a hole is captured by a trapped electron on the lattice site, the self-trapped exciton is produced. Direct or indirect self-trapped exciton emissions are both possible.

In contrast to indirect self-trapped exciton emission, which uses an oxygen vacancy, direct self-trapped exciton emission involves a direct carrier recombination. Since Cu insertion in TiO_2 causes oxygen vacancies to form, oxygen vacancies may be the source of the self-trapped exciton emission at 420 nm. It is related to the change from localized surface states to the valence band of TiO_2 that causes the emission peak at 491 nm (blue emission). Color centers cause peaks at 460 and 535 nm. By introducing additional energy levels to the semiconductor's bandgap, the implanted ions increase the time for electron-hole pairs generated by the photoexcitation process; thus, charge

separation efficiency enhances by irradiation [47]. The low PL intensity suggests a low rate of electron-hole pair recombination, resulting in a high efficiency of the manufactured device. The PL intensity enhances with an increase in Cu^{2+} concentration up to $2x10^{15}$ ions/cm^2. Instead of facilitating charge transfer, the increased concentration of Cu serves as an electron-hole pair recombination center thus resulting decrease of efficiency [45].

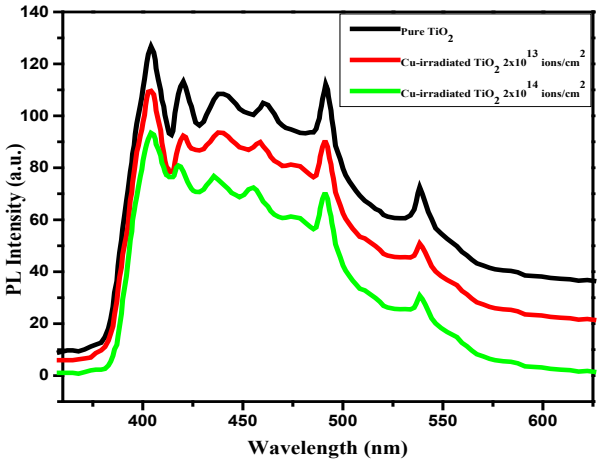

Fig. 6. PL spectrum of pure and Cu-irradiated TiO_2 films.

3.4. Electrochemical impedance spectroscopy

The resistance in the flow of charges in dye-sensitized solar cells can be determined via EIS data [48]. The key parts of dye-sensitized solar cells are TCO, Film, the dye/sensitizer, the redox couple, and the counter electrode. These components' interfaces with one another, such as TCO/Film, Film/dye, sensitizer/redox couple, and redox couple/counter electrode, facilitate the electron-hole pairs recombination, which lowers the device's efficiency. Therefore, device efficiency increases if we are successful in increasing charge injection while reducing their recombination [49].

We used a Nyquist plot of the EIS data to calculate the resistance present in the electron transport at different interfaces. In the impedance curve shown in Figure 7, the first semi-circle describes the resistance in the charges moving through the electrolyte and counter electrode. The middle curve representing the impedance in the electron transport present at TiO_2/dye/electrolyte interfaces. The last semicircle related to the impedance within the electrolyte [50, 51].

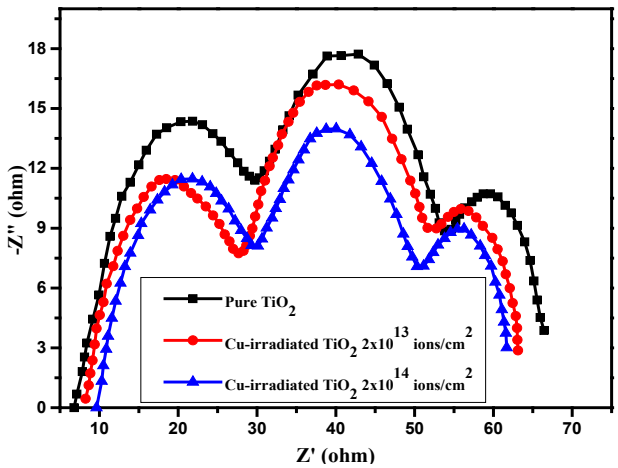

Fig. 7. EIS of pure and Cu-irradiated TiO_2 films.

In the impedance curve, our focus is on the film/dye/electrolyte interface's recombination resistance. Figure 7 shows Nyquist plot of the EIS spectra for TiO_2 exposed to Cu ions and pure TiO_2 at fluency rates of 2 $x10^{13}$ ion/cm^2 and 2 $x10^{14}$ ion/cm^2 respectively. The Nyquist plot is drawn between the two values Z'' and Z', where Z' represents the real impedance, and Z'' the imaginary part. The middle portion of the curve in Figure 7 is our interest. It has been clarified from the Nyquist plot that the semicircle radius reduces with increasing fluency rate when compared to pure TiO_2, demonstrating a reduction of the resistance in the charge transfer at the film/dye/electrolyte interfaces. The lowest resistance is obtained at a fluency rate of 2 $x10^{14}$ ion/cm^2, which is the optimum fluency rate. The low recombination rate and effective charge transfer to TiO_2's conduction band is the cause of the decreased resistance to charge flow. The impurity levels due to Cu ions act as trapping centres, resisting the recombination of electron-hole pairs. The downward shifting of the conduction band with the lowest possible level at 2 $x10^{14}$ ion/cm^2 fluency rate makes it suitable for effective charge transfer, thus facing less resistance in a smooth flow. The efficiency of the developed device drops to 4.90% when the fluency is increased further to 2 $x10^{15}$ ion/cm^2, as this causes an increase in resistance to the smooth flow of charges. Actually, with a high fluency rate of 2 $x10^{15}$ ion/cm^2 of Cu ions, the transparency of the device decreases so, enhances the recombination rate, increasing the resistance of the device [52].

3.5. J-V measurement

For the analysis of DSSCs efficiency, the efficiency formula of DSSC uses open circuit voltage (V_{OC}), short circuit current (J_{SC}), and fill factor (FF) determined from the J-V curve. The following relation is used to compute DSSCs' efficiency[53]

$$\eta(\%) = \frac{J_{SC} \times FF \times V_{OC}}{P_{in}} \times 100 \quad (10)$$

Pin and FF stand for incident light power and fill factor, respectively. J_{SC} is the short circuit current density, while V_{OC} is the open circuit voltage. The device's efficiency is directly related to J_{SC}, V_{OC}, and FF at constant Pin values.

3.5.1. Short circuit current density

The J_{SC} for the pure sample is 8.09 mA/cm^2. When Cu ions were irradiated onto the film at a flow rate of 2 x 10^{13} ions/cm^2, the J_{SC} rose from 8.09 to 8.75mA/cm^2. The value increases to a maximum of 9.32 mA/cm^2 with the fluence rate increasing to 2 x 10^{14} ions/cm^2. This increased short circuit current density J_{SC} value may be credited with incorporating of Cu^{+2} into TiO_2 which improves the electron transfer rate by giving electrons an alternate path, revealing an increase in Jsc [20]. The surface area of TiO_2 was improved by adding Cu^{2+} into the TiO_2 lattice, thus dye loading enhances with a large surface area, so current density Jsc increases; ultimately, the efficiency of DSSC improves [22]. TiO_2 has impurity electron levels of 3d metals, which act as charge traps and slow down the recombination process, increasing the flow rate, thus improvement of photocurrent efficiency of dye-sensitized solar cells is observed. It reveals that adding Cu^{2+} to TiO_2 improves the charge separation efficiency and increases the interfacial charge transfer rate. Implanted Cu^{+2} ions enhance the charge separation time in TiO_2 by adding extra energy levels to the semiconductor bandgap [47].

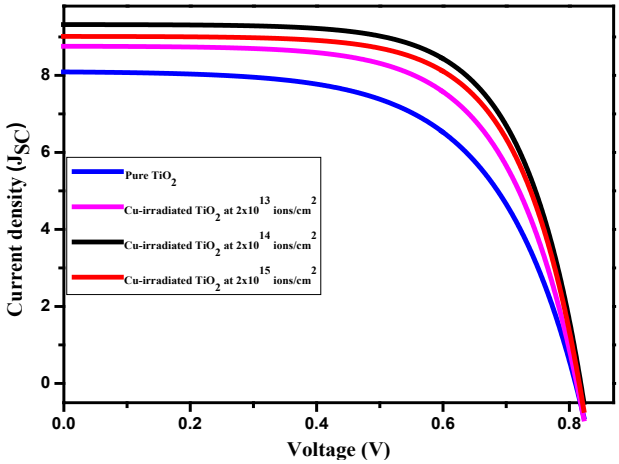

Fig. 8. J-V characteristics of pristine and Cu-irradiated-TiO_2 fabricated DSSCs.

The conduction band gets close to the valance band after Cu ions irradiation is another factor for increasing the short circuit current density [19]. Thus, the charge mobility of Cu irradiated samples increases, so charge recombination decreases, increasing the efficacy of DSSC. At the interface between the electrolyte and counter electrode as well as TiO_2, there was less resistance due to the Cu-irradiation process, and suppression of carrier recombination was considered essential for increasing photo conversion efficiency [54]. On further increasing Cu's fluence rate of 2 x 10^{15} ions/cm^2 in TiO_2, the short circuit current density Jsc decreases to 9.01 mA/cm^2. The lattice structure is damaged at a high fluence rate, increasing the number of crystallographic defects. Additionally, the presence of higher level of copper can result in redox interactions with electrolyte ions that lower Jsc [19]. At higher concentrations of Cu ions, the dye adhesion is negatively affected, so due to aggregation, the absorption area also reduces, and short-circuit current density reduces [55].

3.5.2. Open circuit voltage

The open-circuit voltage (V_{OC}) of a DSSC refers to the voltage that can be measured across the cell's terminals when it is not connected to an external load and is exposed to light to generate a photocurrent. The V_{OC} is an essential parameter in photovoltaic devices, as it represents the maximum voltage that the device can generate under illumination, and it is directly related to the device's energy conversion efficiency. The difference between the photoanode's quasi-Fermi level and the electrolyte's redox potential can be used to compute the photovoltage (V_{OC}). The positive shift in the photoanode's flat band potential (V_{fb}) can be used to explain the decrease in V_{OC}. Equation links the V_{OC} and V_{fb} at the photoanode's quasi-Fermi level.

$$V_{OC} = |V_{fb} - V_{red}| \tag{11}$$

whereas the conduction band position can be calculated by using the following relation [56, 57]

$$V_{fb} = 2.94 - E_g \tag{12}$$

We can infer from the findings that adding Cu basis for the band gap energy to drop in TiO_2. The DSSC's open-circuit voltage has increased due to this drop in Eg, as seen in relation 12. The reduced band gap value is the reason for the improvement in the open circuit voltage [58, 59]. The enhancement of V_{OC} is brought about by a reduction in V_{fb} due to the interaction of Cu^{2+} with the defect state. V_{OC} is related to the band gap energy, as seen in equations 11 and 12, so its variations are similar to band gap energy. Thus, the open circuit voltage drops to 0.8182 V as the band gap energy increases to 2 x 10^{15} ions/cm^2. After irradiating the TiO_2 film with Cu ions at a flux rate of 2x10^{13} ions/cm^2, the fill factor likewise improved, rising from 0.5981 to 0.6402. As the Cu^{2+} fluence

rate approaches $2x10^{14}$ ions/cm^2, this rises to 0.6706 and decreases to 0.6635 when the flow rate hits $2x10^{15}$ ions/cm^2. The high value of FF is evidence that the recombination rate has been reduced, which ultimately improves the device's efficiency [60]. Suppressing the reverse electron transfer can increase V_{OC} and FF.[61]. The highest efficiency of 5.10% is achieved by these modifications in TiO_2 film with Cu^{+2}.

Table 3. Solar cells parameters.

Samples	Jsc (mA/cm^2)	Voc (V)	FF	Efficiency η (%)
Pure TiO_2	8.09	0.8099	0.5981	3.92
Cu ($2x10^{13}$) irradiated-TiO_2	8.75	0.8117	0.6402	4.55
Cu ($2x10^{14}$) irradiated-TiO_2	9.32	0.8158	0.6706	5.10
Cu ($2x10^{15}$) irradiated-TiO_2	9.01	0.8182	0.6635	4.90

4. Conclusion

In this study, we employed 700 keV Cu^{+2} ions with fluence rates of $2x10^{13}$, $2x10^{14}$, and $2x10^{15}$ ions/cm^2 to implant them into TiO_2 films. X-ray Diffraction (XRD) analysis verified the presence of the anatase phase in both the pure and Cu-irradiated samples. Interestingly, a reduction in the average crystallite size was observed specifically at the fluence rate of $2x10^{14}$ ions/cm^2. Moreover, Cu implantation caused variations in the band gap energy (Eg), with the lowest Eg recorded at the same $2x10^{14}$ ions/cm^2 fluence rate. At this fluency rate, a study of photoluminescence (PL) spectra showed a decrease in defective peaks, suggesting enhanced material quality. Additional data was acquired through the application of electrochemical impedance spectroscopy (EIS), which verified that the interface between the film, dye, and electrolyte exhibited the least resistance when subjected to the $2x10^{14}$ ions/cm^2 fluence rate. This decrease in resistance improves charge carrier transport across these interfaces, thus increasing the effectiveness of the photovoltaic system. The dye-sensitized solar cell fabricated using a modified anode with Cu ions at a $2x10^{14}$ ions/cm^2 fluence rate shows exceptional performance. The high short-circuit current density Jsc (9.32 mA/cm^2) and FF (0.67) result in a maximum photoconversion efficiency of 5.10%. These observations highlighted the significance of the ion implantation method to modify TiO_2 film for modern solar energy uses.

References

[1] K. Fan, J. Yu, W. Ho, Materials Horizons, vol. 4, pp. 319-344, 2017; https://doi.org/10.1039/C6MH00511J

[2] Y. Shang, S. Hao, C. Yang, G. Chen, Nanomaterials, vol. 5, pp. 1782-1809, 2015; https://doi.org/10.3390/nano5041782

[3] J. Gong, K. Sumathy, Q. Qiao, Z. Zhou, Renewable and Sustainable Energy Reviews, vol. 68, pp. 234-246, 2017; https://doi.org/10.1016/j.rser.2016.09.097

[4] B. O'regan, M. Grätzel, Nature, vol. 353, pp. 737-740, 1991; https://doi.org/10.1038/353737a0

[5] Y. Ren, D. Zhang, J. Suo, Y. Cao, F. T. Eickemeyer, N. Vlachopoulos, S. M. Zakeeruddin, A. Hagfeldt, M. Grätzel, Nature, pp. 1-3, 2022; https://doi.org/10.1038/s41586-022-05460-z

[6] J. Chae, D. Y. Kim, S. Kim, M. Kang, Journal of industrial and Engineering Chemistry, vol. 16, pp. 906-911, 2010; https://doi.org/10.1016/j.jiec.2010.09.012

[7] D. Kuang, C. Klein, S. Ito, J. E. Moser, R. Humphry-Baker, N. Evans, F. Duriaux, C. Graetzel, S. M. Zakeeruddin, M. Grätzel, Advanced Materials, vol. 19, pp. 1133-1137, 2007; https://doi.org/10.1002/adma.200602172

[8] Q. Wang, S. Ito, M. Grätzel, F. Fabregat-Santiago, I. Mora-Sero, J. Bisquert, T. Bessho, H. Imai, The Journal of Physical Chemistry B, vol. 110, pp. 25210-25221, 2006; https://doi.org/10.1021/jp064256o

[9] H. Siddiqui, Ion Beam Techniques and Applications, ed: IntechOpen, 2019; https://doi.org/10.5772/intechopen.83566

[10] D. Chu, X. Yuan, G. Qin, M. Xu, P. Zheng, J. Lu, L. Zha, Journal of Nanoparticle Research, vol. 10, pp. 357-363, 2008; https://doi.org/10.1007/s11051-007-9241-7

[11] T. Ohno, M. Akiyoshi, T. Umebayashi, K. Asai, T. Mitsui, M. Matsumura, Applied Catalysis A: General, vol. 265, pp. 115-121, 2004; https://doi.org/10.1016/j.apcata.2004.01.007

[12] G. R. Torres, T. Lindgren, J. Lu, C.-G. Granqvist, S.-E. Lindquist, The Journal of Physical Chemistry B, vol. 108, pp. 5995-6003, 2004; https://doi.org/10.1021/jp037477s

[13] A. Yella, H.-W. Lee, H. N. Tsao, C. Yi, A. K. Chandiran, M. K. Nazeeruddin, E. W.-G. Diau, C.-Y. Yeh, S. M. Zakeeruddin, M. Grätzel, Science, vol. 334, pp. 629-634, 2011; https://doi.org/10.1126/science.1209688

[14] M. Ye, C. Chen, M. Lv, D. Zheng, W. Guo, C. Lin, Nanoscale, vol. 5, pp. 6577-6583, 2013; https://doi.org/10.1039/c3nr01604h

[15] A. Stepanov, Rev. Adv. Mater. Sci, vol. 30, pp. 150-165, 2012.

[16] M. Dhonde, K. Sahu, V. Murty, Solar Energy, vol. 220, pp. 418-424, 2021; https://doi.org/10.1016/j.solener.2021.03.072

[17] S. Shakir, Z. S. Khan, A. Ali, N. Akbar, W. Musthaq, Journal of Alloys and Compounds, vol. 652, pp. 331-340, 2015; https://doi.org/10.1016/j.jallcom.2015.08.243

[18] M. H. Haji Jumali, R. R. Noor, M. Yahaya, M. M. Salleh, A. A. Umar, Advanced Materials Research, 2012, pp. 485-488; https://doi.org/10.4028/www.scientific.net/AMR.364.485

[19] L. Zhou, L. Wei, Y. Yang, X. Xia, P. Wang, J. Yu, T. Luan, Chemical Physics, vol. 475, pp. 1-8, 2016; https://doi.org/10.1016/j.chemphys.2016.05.018

[20] L. Patle, V. Huse, A. Chaudhari, Materials Research Express, vol. 4, p. 105045, 2017; https://doi.org/10.1088/2053-1591/aa919a

[21] T. Raguram, K. Rajni, Applied Physics A, vol. 125, pp. 1-11, 2019; https://doi.org/10.1007/s00339-019-2581-1

[22] S. Chahid, D. M. de los Santos, R. Alcántara, Proceedings of the 3rd International Conference on Smart City Applications, 2018, pp. 1-10; https://doi.org/10.1145/3286606.3286854

[23] R. Karmakar, S. Neogi, A. Banerjee, S. Bandyopadhyay, Applied surface science, vol. 263, pp. 671-677, 2012; https://doi.org/10.1016/j.apsusc.2012.09.133

[24] S. Fujihara, C. Sasaki, T. Kimura, Journal of the European Ceramic Society, vol. 21, pp. 2109-2112, 2001; https://doi.org/10.1016/S0955-2219(01)00182-0

[25] R. W. Kelsall, I. W. Hamley, M. Geoghegan, Nanoscale Science and Technology, 2005; https://doi.org/10.1002/0470020873

[26] S. Neogi, S. Chattopadhyay, A. Banerjee, S. Bandyopadhyay, A. Sarkar, R. Kumar, Journal of Physics: Condensed Matter, vol. 23, p. 205801, 2011; https://doi.org/10.1088/0953-8984/23/20/205801

[27] M. Khan, Results in physics, vol. 7, pp. 3176-3180, 2017; https://doi.org/10.1016/j.rinp.2017.08.038

[28] M. Irfan, M. Khan, M. Amami, R. Ahson, E. A. Alabbad, Optical Materials, vol. 123, p. 111794, 2022; https://doi.org/10.1016/j.optmat.2021.111794

[29] T. Raguram, K. Rajni, Journal of Materials Science: Materials in Electronics, vol. 32, pp. 18264-18281, 2021; https://doi.org/10.1007/s10854-021-06369-5

[30] H. Sokoidanto, A. Taufik, R. Saleh, Journal of Physics: Conference Series, 2020, p. 012008; https://doi.org/10.1088/1742-6596/1442/1/012008

[31] S. Thogiti, J. Y. Park, C. T. Thanh Thuy, D. K. Lee, B.-K. Min, H. J. Yun, J. H. Kim, ACS Sustainable Chemistry & Engineering, vol. 6, pp. 13025-13034, 2018; https://doi.org/10.1021/acssuschemeng.8b02543

[32] J. Navas, C. Fernández-Lorenzo, T. Aguilar, R. Alcántara, J. Martín-Calleja, physica Status Solidi A, vol. 209, pp. 378-385, 2012; https://doi.org/10.1002/pssa.201127336

[33] A. Suresh, N. Soundararajan, A. Ahmed, Int. J. Chem. Tech. Res, vol. 524, 2014.

[34] S. K. M. Saad, A. A. Umar, M. Y. A. Rahman, M. M. Salleh, Applied Surface Science, vol. 353, pp. 835-842, 2015; https://doi.org/10.1016/j.apsusc.2015.06.181

[35] J. Mohapatra, D. Mishra, S. Kamilla, V. Medicherla, D. Phase, V. Berma, S. Singh, Physica Status Solidi B, vol. 248, pp. 1352-1359, 2011; https://doi.org/10.1002/pssb.201046513

[36] S. Roy, A. Bhuiyan, Sensors & Transducers, vol. 195, p. 18, 2015.

[37] T.-T. Pham, C. Nguyen-Huy, H.-J. Lee, T.-D. Nguyen-Phan, T. H. Son, C.-K. Kim, E. W. Shin, Ceramics International, vol. 41, pp. 11184-11193, 2015; https://doi.org/10.1016/j.ceramint.2015.05.068

[38] S. Wang, S. Han, G. Xin, J. Lin, R. Wei, J. Lian, K. Sun, X. Zu, Q. Yu, Materials & Design, vol. 139, pp. 181-187, 2018; https://doi.org/10.1016/j.matdes.2017.11.010

[39] J. Rotich, M. Mwamburi, N. Walter, C. Maghanga, O. Munyati, S. Hatwaambo, Materials Research Express, vol. 7, p. 025505, 2020; https://doi.org/10.1088/2053-1591/ab6e29

[40] F. Shan, G. Liu, W. Lee, G. Lee, I. Kim, B. Shin, Y. Kim, Journal of crystal growth, vol. 277, pp. 284-292, 2005; https://doi.org/10.1016/j.jcrysgro.2005.01.016

[41] M. H. Samat, N. Hussin, M. F. M. Taib, M. K. Yaakob, N. S. Samsi, S. S. S. A. Aziz, M. Yahya, A. Ali, Materials Science Forum, 2016, pp. 726-733; https://doi.org/10.4028/www.scientific.net/MSF.846.726

[42] M. Islam, J. Podder, Crystal Research and Technology: Journal of Experimental and Industrial Crystallography, vol. 44, pp. 286-292, 2009; https://doi.org/10.1002/crat.200800326

[43] L. Li, J. Liu, Y. Su, G. Li, X. Chen, X. Qiu, T. Yan, Nanotechnology, vol. 20, p. 155706, 2009; https://doi.org/10.1088/0957-4484/20/15/155706

[44] G. Liu, C. Sun, X. Yan, L. Cheng, Z. Chen, X. Wang, L. Wang, S. C. Smith, G. Q. M. Lu, H.-M. Cheng, Journal of Materials Chemistry, vol. 19, pp. 2822-2829, 2009; https://doi.org/10.1039/b820816f

[45] Y. Li, X. Zhou, W. Chen, L. Li, M. Zen, S. Qin, S. Sun, Journal of hazardous materials, vol. 227, pp. 25-33, 2012; https://doi.org/10.1016/j.jhazmat.2012.04.071

[46] K. Amarsingh Bhabu, A. Kalpana Devi, J. Theerthagiri, J. Madhavan, T. Balu, T. Rajasekaran, Journal of Materials Science: Materials in Electronics, vol. 28, pp. 3428-3439, 2017; https://doi.org/10.1007/s10854-016-5940-0

[47] N. Smirnova, I. Petrik, V. Vorobets, G. Kolbasov, A. Eremenko, Nanoscale Research Letters, vol. 12, pp. 1-8, 2017; https://doi.org/10.1186/s11671-017-2002-3

[48] S. Sarker, H. W. Seo, D.-W. Seo, D. M. Kim, Journal of Industrial and Engineering Chemistry, vol. 45, pp. 56-60, 2017; https://doi.org/10.1016/j.jiec.2016.09.002

[49] L. Yang, B.-g. Zhai, Q.-l. Ma, Y. M. Huang, Journal of Alloys and Compounds, vol. 605, pp. 109-112, 2014; https://doi.org/10.1016/j.jallcom.2014.03.118

[50] N. Koide, A. Islam, Y. Chiba, L. Han, Journal of Photochemistry and Photobiology A: chemistry, vol. 182, pp. 296-305, 2006; https://doi.org/10.1016/j.jphotochem.2006.04.030

[51] L. Han, N. Koide, Y. Chiba, T. Mitate, Applied Physics Letters, vol. 84, pp. 2433-2435, 2004; https://doi.org/10.1063/1.1690495

[52] T. Sakthivel, K. A. Kumar, R. Ramanathan, J. Senthilselvan, K. Jagannathan, Materials Research Express, vol. 4, p. 126310, 2017; https://doi.org/10.1088/2053-1591/aa9e36

[53] H.-C. Lin, H.-S. Chen, C.-Y. Su, C. Su, 2009 34th IEEE Photovoltaic Specialists Conference (PVSC), 2009, pp. 000907-000910; https://doi.org/10.1109/PVSC.2009.5411141

[54] D. Dahlan, S. K. M. Saad, A. U. Berli, A. Bajili, A. A. Umar, Physica E: Low-dimensional Systems and Nanostructures, vol. 91, pp. 185-189, 2017; https://doi.org/10.1016/j.physe.2017.05.003

[55] K. Sahu, M. Dhonde, V. V. S. Murty, International Journal of Energy Research, vol. 45, pp. 5423-5432, 2021; https://doi.org/10.1002/er.6169

[56] S. Iwamoto, Y. Sazanami, M. Inoue, T. Inoue, T. Hoshi, K. Shigaki, M. Kaneko, A. Maenosono, ChemSusChem: Chemistry & Sustainability Energy & Materials, vol. 1, pp. 401-403, 2008; https://doi.org/10.1002/cssc.200700163

[57] C. Zhang, S. Chen, L. e. Mo, Y. Huang, H. Tian, L. Hu, Z. Huo, S. Dai, F. Kong, X. Pan, The Journal of Physical Chemistry C, vol. 115, pp. 16418-16424, 2011; https://doi.org/10.1021/jp2024318

[58] A. Supriyanto, W. Obina, T. Septiawan, A. Ramelan, F. Nurosyid, Journal of Physics: Conference Series, 2019, p. 012048; https://doi.org/10.1088/1742-6596/1170/1/012048

[59] A. A. Qureshi, S. Javed, H. M. A. Javed, A. Akram, M. Jamshaid, A. Shaheen, Optical Materials, vol. 109, p. 110267, 2020; https://doi.org/10.1016/j.optmat.2020.110267

[60] M. Khan, N. Fatima, G. M. Mustafa, M. Sabir, S. A. Abubshait, H. A. Abubshait, T. Alshahrani, M. Iqbal, A. Laref, M. Baig, International Journal of Energy Research, vol. 45, pp. 9685-9693, 2021; https://doi.org/10.1002/er.6469

[61] H. Tian, L. Hu, C. Zhang, W. Liu, Y. Huang, L. Mo, L. Guo, J. Sheng, S. Dai, The Journal of Physical Chemistry C, vol. 114, pp. 1627-1632, 2010; https://doi.org/10.1021/jp9103646